

Inferring the Dynamics of Ground-State Evolution of Quantum Annealers

Elijah Pelofske, Georg Hahn, and Hristo Djidjev

Los Alamos National Laboratory

Abstract

To solve an optimization problem using a commercial quantum annealer, one has to represent the problem of interest as an Ising or a quadratic unconstrained binary optimization (QUBO) problem and submit its coefficients to the annealer, which then returns a user-specified number of low-energy solutions. It would be useful to know what happens in the quantum processor during the anneal process so that one could design better algorithms or suggest improvements to the hardware. However, existing quantum annealers are not able to directly extract such information from the processor. Hence, in this work we propose to use advanced features of the newest annealer generation, the D-Wave 2000Q, to indirectly infer information about the dynamics of the ground-state during the anneal process. Specifically, D-Wave 2000Q allows the user to customize the anneal schedule, that is, the schedule with which the anneal fraction is changed from the start to the end of the anneal. Using this feature, we design a set of modified anneal schedules whose outputs can be used to generate information about the states of the system at user-defined time points during a standard anneal. With this process, called *slicing*, we obtain approximate distributions of lowest-energy anneal solutions as the anneal time evolves. We use our technique to obtain a variety of insights into the annealer such as how the ground state evolves during the annealing, when individual bits in an evolving solution flip during the anneal process and when they stabilize, and we introduce an approximate technique to determine the freeze-out point of the system as well as of individual qubits.

1 Introduction

Quantum computers of D-Wave Systems, Inc., use a process called *quantum annealing* to quickly obtain approximate solutions of very high quality for NP-hard problems [4]. The type of function that the D-Wave annealer is designed to minimize is given by

$$Q(q_1, \dots, q_n) = \sum_{i=1}^n a_i q_i + \sum_{i \leq j} a_{ij} q_i q_j, \quad (1)$$

where $n \in \mathbb{N}$ is the number of variables, $a_i \in \mathbb{R}$ are the linear weights, and $a_{ij} \in \mathbb{R}$ are the quadratic weights. If $q_i \in \{-1, +1\}$, the function in (1) is called an *Ising* model. If $q_i \in \{0, 1\}$, it is called a quadratic unconstrained binary optimization (*QUBO*) model. The two formulations are equivalent since they can be converted into each other by a linear transformation of the

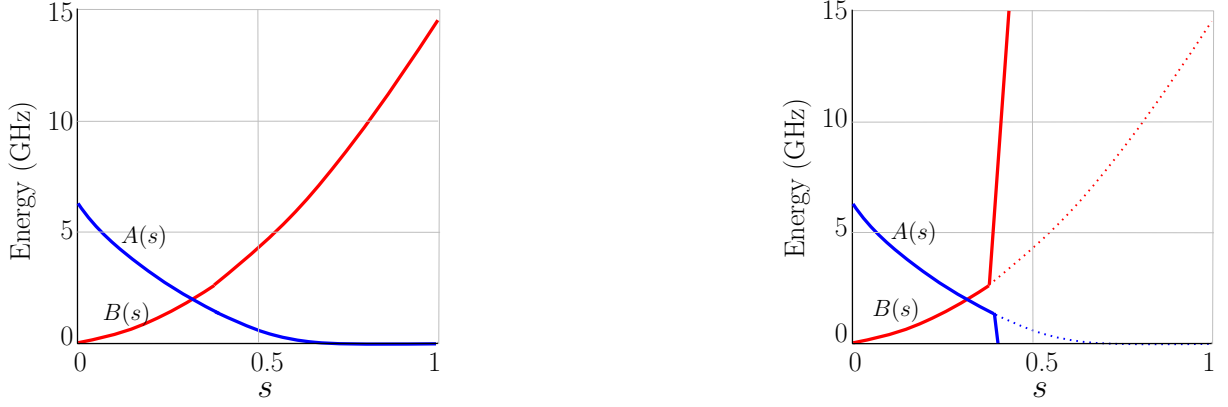


Figure 1: Left: Functions $A(s)$ (blue) and $B(s)$ (red) for D-Wave 2000Q, where $s \in [0, 1]$ is the annealing fraction in a regular schedule [5]. Right: Functions $A(s)$ and $B(s)$ in a quenching schedule.

variables, and we consider both QUBO and Ising models in this work. Many important NP-complete problems, such as the maximum clique, minimum vertex cover, and the graph coloring problem, can be expressed as a minimization of the form (1) [18, 3, 19, 8, 9].

We typically apply the following three steps in order to implement and solve an NP-hard problem on the D-Wave annealer. First, we express the problem under investigation as a minimization of type (1). Second, the coefficients a_i and a_{ij} of the instance of (1) we want to solve are mapped onto the qubits and the connections between them (called *couplers*) of the D-Wave chip [6]. Third, a pre-specified number of reads (solutions) are requested from the D-Wave annealer. In particular, for each read, the value of the i -th variable is given as the i -th bit of a bitstring which D-Wave returns as its output from the read.

An operator called *Hamiltonian* describes the time evolution of any quantum system. For the D-Wave processor, the following time-dependent Hamiltonian specifies its quantum system evolution:

$$H(s) = -\frac{A(s)}{2} \sum_{i=1}^n \sigma_i^x + \frac{B(s)}{2} \left(\sum_{i=1}^n a_i \sigma_i^z + \sum_{i \leq j} a_{ij} \sigma_i^z \sigma_j^z \right).$$

In $H(s)$, the first term imposes an equal superposition of all states, i.e., such that each output bit string is equally likely. The actual input problem, determined by the coefficients a_i and a_{ij} from (1), is encoded in the second term. A so-called *anneal path* handles how the quantum system transitions from the initial quantum state to the final one, by specifying the functions $A(s)$ and $B(s)$. Figure 1 (left) displays the values of these functions for the D-Wave 2000Q machine at Los Alamos National Laboratory. Both functions are indexed by a parameter $s \in [0, 1]$ called the *anneal fraction*. Importantly, at the end of the anneal, we have $s = 1$ and $A(s) = 0$, meaning that the final Hamiltonian $H(1)$ is associated with a low-energy quantum system whose qubits' values can be measured to get a high-quality solution of (1).

The newest model of D-Wave annealers, 2000Q, gives more freedom to the user to tune some of the annealing control parameters [7]. Such options include a server-side spin reversal [17], pausing [11], reverse annealing schedules [14], and time-dependent gain in linear biases [20]. Using up to 50 points, the *anneal schedule* specifies how the anneal fraction evolves from the start to the end of the anneal [6, Figure 2.1]. Previously, this feature has been used for improving

the accuracy of the annealer by inserting a pause in the anneal schedule [11, 15].

The aim of this article is to investigate how the quantum state of the D-Wave annealer changes during an anneal process. This process is unobservable directly, since D-Wave only allows users to read off the final qubit states at the end of each anneal. For this reason, we design a set of modified anneal schedules whose outputs can be used to generate information about the states of the system at user-defined time points during a standard anneal. Using a custom anneal schedule and *quenching*, a standard feature provided by D-Wave 2000Q [6, Section 2.5.2], we follow the usual anneal curve up to a specific time at which we would like to obtain information about the state. We then modify the anneal schedule by inserting a jump to the full anneal (see Figure 1, right), thus getting a snapshot of the state at that intermediate time point. Repeating this technique for various intermediate points allows us to *slice* the anneal and then stitch all the information together in order to gain better understanding about the dynamics of the anneal process.

We employ our technique to obtain some insights of D-Wave’s anneal process which, to the best of our knowledge, have not been reported previously in the literature. First, our approach allows us to visualize how the ground state evolves during the anneal process, both in terms of its energy and in terms of its dynamics, that is, we measure how volatile the measured value of each individual qubit of the lowest energy state is during the anneal. We repeat those experiments for a varying number of slices and annealing times.

Second, in order to better understand what happens during an anneal, we present a simple genetic optimization scheme [12] designed to find a QUBO that exhibits substantial improvements in terms of energy decrease. We contrast the (optimized) QUBO obtained in this fashion with a random QUBO. Moreover, we study the characteristics and best parameter choices for our genetic algorithm.

Third, our technique gives us a new way to determine the *freezeout point*, a hypothetical point that is defined as an anneal fraction s significantly smaller than 1, after which the dynamics essentially stalls, and which can be found by fitting a Boltzmann distribution to the annealer’s output. While we show that a freezeout point so defined may not always exist or be identifiable by the existing methods, we demonstrate that our slicing method allows us to determine an analogue we call a *quasi-freezeout point (QFP)*. It is defined as a point at which either the energy does not significantly improve anymore or, at an individual qubit level, a point at which the state/value of each individual qubit stays fixed. For the former, we analyze the energy values determined by the slicing method and determine the point after which the slope of the energy plot becomes close to zero. We compare our approach to the one based on estimating the parameters of a Boltzmann distribution, e.g., [2]. For the latter, qubit-level QFP, we slice the anneal at various stages (for instance, using 1000 slices for a 1000 microsecond anneal), and observe how each qubit’s measured value (+1 or 0/−1) changes over the course of the anneal. The QFP of a qubit can then be defined as the approximate location at which the measured value of the qubit stays invariant until the end of the anneal.

The article is structured as follows. Section 2 presents our approach to slice the anneal process, that is, the anneal schedule we employ in order to quench the anneal process at any intermediate time. We also present our genetic algorithm to find a QUBO for which the ground

state exhibits a substantial change during the anneal, both in terms of the total number of bit flips of all involved qubits, as well as the total energy decrease during the anneal. Using that QUBO, Section 3 will visualize how the ground state evolves during the anneal, both in terms of the number of bit flips and the total energy change. We investigate how a random QUBO compares to our optimized one, and how the number of slices influences the results. Finally, we look at freezeout point measurements for various examples. A summary and discussion of our methodology and results can be found in Section 4.

This paper is a journal version of an article presented at the *20th International Conference on Parallel and Distributed Computing, Applications and Technologies (PDCAT) 2019* [16]. Extending the conference version, the present paper also considers the calculation of the freezeout point based on estimation of effective temperatures (Section 2.3) and on information collecting during the slicing (Section 3.7), and we consider schedules that use a pause during the the annealing (Section 2.4). Additionally, the present paper contains more extensive experiments investigating the effect of a pause in the anneal process (Section 3.5), and the slicing of a QUBO for the Maximum Clique problem (Section 3.6), a well-known NP-hard problem. Since the connectivity structure (the quadratic couplers) of the function of type (1) being minimized on D-Wave does typically not match the one of the physical qubits on the D-Wave chip, one important aspect of quantum annealing pertains to the computation of a suitable minor embedding of the problem structure in (1) onto the physical qubits. In this process, logical qubits are often represented as a set of physical ones that are supposed to act as one (called a "chain"). Even though chains of physical qubits represent the same logical qubit, it is not guaranteed that all of them take the same value after readout at the end of the anneal. This is called a "broken chain". We visualize how chain breaks occur during the anneal (Section 3.8) and visualize the freezeout points for all individual qubits (Section 3.9). Finally, most of the figures are new or revised, compared to the conference version.

2 Methodology

This section, which presents the methodology underlying our work, consists of two parts. First, Section 2.1 describes the quenching technique we use in order to get information about the ground state evolution during the anneal process. To visualize results later in the simulations, we are interested in finding a QUBO that exhibits a pronounced evolution during the anneal process, that is, whose lowest energy result from a 1-microsecond D-Wave anneal is (significantly) greater than that of a longer (1000-microsecond) anneal. We find such a QUBO with the help of a genetic algorithm presented in Section 2.2. This section ends with a review of a published technique to estimate freezeout points using the technique of [2] in Section 2.3, and a short discussion of how to slice an anneal schedule with a pause in Section 2.4.

2.1 Slicing the anneal process

The goal of this work is to investigate how the ground state evolves during the anneal process of D-Wave 2000Q. For this, we use a feature recently introduced for the D-Wave machines: it allows users to manually define an anneal schedule through the specification of up to 50 points

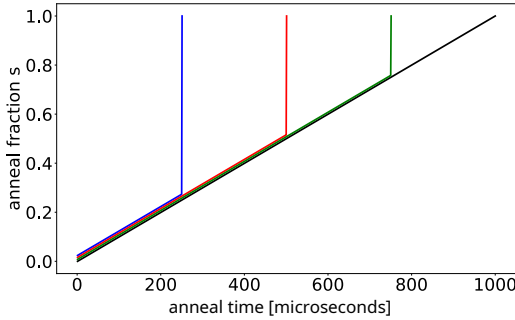


Figure 2: Anneal schedule with quenching (near-vertical jumps) at time points 250 (blue), 500 (red), and 750 (green) microseconds. Total anneal time of 1000 microseconds. The full anneal schedule is shown by the black line.

on the anneal curve. In particular, we make use of a feature called ”quenching”, which allows us to jump to the full anneal fraction of 1 within one microsecond at any point in the anneal (for the precise conditions under which the quench is possible, see [6]).

Figure 2 illustrates the sequences of quenches we employ. For the i -th quench, in order to slice the anneal process at time t_i , we follow the standard anneal curve connecting point $P_0 = (0, 0)$, meaning $t = 0$ and $s = 0$, with point with $P_1 = (t_i, t_i)$ by a segment, and then connecting P_1 by a segment to point $P_2 = (t_i + 1, 1)$. Ideally, the jump from an intermediate anneal fraction to the end of the anneal has to be done as quickly as possible, i.e., we would like to have $P_2 = (t_i, 1)$ in order to “freeze” the ground state information at time t_i . But due to the hardware constraints of D-Wave 2000Q for specifying the anneal curve, precisely, that the maximal degree of the anneal curve should not exceed 45 degrees, this is not possible.

Though the jump we employ is not perfectly vertical (our anneal curve jumps to 1 at $t_i + 1$), we expect this jump to not considerably change the result. But we also would like to reduce the bias caused by the $1\mu s$ quench, since for some problems $1\mu s$ anneal could reduce noticeably the energy of the ground state. Hence, in the next subsection, we discuss our approach to choosing problems for which the distortion caused by the quench is significantly reduced.

2.2 A genetic algorithm for constructing a suitable QUBO/Ising model

It is known that different QUBO/Ising models pose different levels of difficulty to the D-Wave annealer when it comes to finding a high quality solution [3]. In our experiments presented in Section 3, we aim to investigate how the ground state evolves during the anneal process, and therefore seek to solve a non-trivial QUBO/Ising instance for which the effect of quenching is as small as possible, and and that also exhibits a distinctive evolution measured both in terms of energy decrease and bit flips during the anneal process.

To find such a problem instance, we employ the genetic algorithm presented in Algorithm 1, which works as follows. The algorithm starts by initializing a population of $N \in \mathbb{N}$ problem instances (QUBO or Ising models), which are collected in a set S . Those instances are randomly generated as follows: each problem instance maps onto the entire Chimera graph, the graph encoding the connectivity structure of the physical qubits on the D-Wave chip, see [6]. Its linear coefficients a_i are independently sampled from $(-2, 2)$, and its quadratic coefficients a_{ij} are

Algorithm 1: Finding a suitable QUBO/Ising model for slicing

```
input  :  $N, p_{\text{cross}}, p_{\text{mut}}, R$ ;  
output: optimized instance for slicing;  
1  $S \leftarrow \{Q_1, \dots, Q_N\}$ , where each  $Q_i$  contains all linear and quadratic terms of the  
   hardware connectivity graph;  
2 for each  $Q \in S$  do  
3   | Set each individual linear coefficient of  $Q$  to a random value in  $(-2, 2)$ ;  
4   | Set each quadratic coefficient of  $Q$  to a random value in  $(-1, 1)$ ;  
5 end  
6 repeat  $R$  times  
7   | for each  $Q \in S$  do  
8   |   | Across 1000 anneals, find energy difference  $\Delta$  between the 1% minimum energy  
9   |   | samples for  $Q$  for a 1 microsecond and 1000 microsecond full anneal;  
10  |   | Set fitness  $f_Q \leftarrow \Delta$ ;  
11  | end  
12  |  $F_0 \leftarrow$  proportion  $p_{\text{cross}}$  of largest  $f_Q$  values;  
13  |  $S_0 \leftarrow \{Q \in S : f_Q \in F_0\}$ ;  
14  |  $S_1 \leftarrow \emptyset$ ;  
15  | repeat  $N$  times  
16  |   | Draw two random  $Q_1, Q_2 \in S_0$  and select coefficients randomly from either  $Q_1$  or  
17  |   |  $Q_2$  with probability 0.5; store new problem instance in  $S_1$ ;  
18  | end  
19  |  $S_2 \leftarrow \emptyset$ ;  
20  | for  $Q \in S_1$  do  
21  |   | Overwrite each coefficient in  $Q$  independently with probability  $p_{\text{mut}}$  (for linear  
22  |   | coefficients use random value in  $(-2, 2)$ , for quadratic coefficients use  $(-1, 1)$ );  
23  |   | store mutated  $Q$  in  $S_2$ ;  
24  | end  
25  |  $S \leftarrow S_2$ ;  
26 end  
27 return fittest  $Q \in S$  as defined in line 9;
```

independently sampled from $(-1, 1)$.

Then the algorithm proceeds by evaluating the fitness of the current population of problem instances. To this end, for each $Q \in S$, we find the mean of the best 1 percent energies in a 1 microsecond and a 1000 microsecond anneal. We set the fitness f_Q for each $Q \in S$ to $|f_{Q,1} - f_{Q,1000}|$, where $f_{Q,1}$ is the average of the best 1% samples from the 1 microsecond anneal, and $f_{Q,1000}$ is the average of the best 1% samples from the 1000 microsecond anneal. Using the mean of the best 1% samples results in more stable results and reduces the effect of the noise, compared to merely considering the minimum energy. The objective function f_Q ensures that Algorithm 2.2 will optimize for problem instances having the property that between a 1 microsecond and a full 1000 microsecond anneal, the ground state evolves considerably in terms of the energy.

Next, the p_{cross} portion of fittest individuals are selected from the population for cross-over and mutation. Those problem instances are stored in the set S_0 . Then we restore the original size N of the population by crossing the fittest individuals from set S_0 : we randomly choose two instances Q_1 and Q_2 from S_0 and generate a new one by selecting each individual linear and quadratic coefficient independently from either Q_1 or Q_2 with probability 0.5. We store the new instance in S_1 and repeat this step N times.

Finally, a mutation step is applied to the new population. For each instance $Q \in S_1$ from the new population, we overwrite any of the coefficients of Q with probability p_{mut} . As in the initialization step, a linear coefficient is sampled randomly from $(-2, 2)$ and a quadratic coefficient is sampled from $(-1, 1)$. The unmutated and mutated instances are stored in a new set S_2 . After setting $S \leftarrow S_2$, the genetic algorithm is restarted with the newest population.

The entire process is repeated over R iterations. After the last iteration, we return the fittest $Q \in S$ as the result of our algorithm, where S is the newest population generation and fitness is calculated as f_Q .

The dependence of the genetic algorithm described in Section 2.2 on its parameters is evaluated in Section 3.1, where we also suggest default parameter choices.

2.3 Estimating the freezeout point

The slicing methodology we introduce in Section 2.1 allows one to track how the ground state, in particular its associated energy, evolves during the anneal process. A natural parameter to look at in this scenario is the so-called *freezeout point* [1, 10], defined as a point before the end of the anneal at which the evolution of the quantum state “freezes” and after which not much quantum dynamics occurs except for fluctuations due to noise. While such a freezeout point may not always be well-defined theoretically or easy to compute, our slicing method gives an alternative way to look at the evolution of the anneal process than those published in the literature. Overall, we are interested in determining a point at which the dynamics of the anneal process slows down or stops.

In order to be able to make a comparison, we want to compute the freezeout point based on an established technique such as [1] or [10], and then compare it with the freezeout point computed by our method.

We use the statistical methodology of [2] to estimate the freezeout point. This method

is based on the Boltzmann distribution, the theoretical distribution of ground-state energies of the annealer. Briefly, estimating a certain parameter of the Boltzmann distribution, the effective inverse temperature β_{eff} of the annealer, allows one to compute the freezeout point. First, we observe that the (thermodynamical) probability of observing an energy E is given by $P_\beta(E) = g(E) \exp(-\beta E)/Z(\beta)$, where $g(E)$ is the degeneracy of the energy level E and $Z(\beta)$ is the partition function serving as normalization factor.

Second, for two energies E_1 and E_2 , the log ratio of probabilities is then

$$l(\beta) := \log \frac{P_\beta(E_1)}{P_\beta(E_2)} = \log \frac{g(E_1)}{g(E_2)} - \beta \Delta E.$$

The main idea of [2] is to rescale all coefficients of the Hamiltonian under consideration by a factor $x \in (0, 1)$. Denoting $\beta = \beta_{\text{eff}}$ and $\beta' = x\beta_{\text{eff}}$, computing the difference of log probabilities then allows us to eliminate the unknown degeneracies $g(\cdot)$ since

$$\Delta l = \frac{P_\beta(E_1)P_{\beta'}(E_2)}{P_\beta(E_2)P_{\beta'}(E_1)} = \Delta\beta\Delta E. \quad (2)$$

The expression in (2) allows us to empirically compute the freezeout point. Indeed, for a fixed $x \in (0, 1)$, we rescale our Hamiltonian under consideration and obtain a fixed number of R anneals for both the unscaled (original) and rescaled Hamiltonians. By binning the obtained energies of those R anneals per Hamiltonian, we can compute empirical probabilities for each energy bin. Using $K = \lceil \sqrt{2R} \rceil$ bins is recommended in [2]. Afterwards, we can select all pairs of bins for both Hamiltonians and compute both Δl and ΔE per pair. According to (2), the data pairs $(\Delta l, \Delta E)$ will lay on a straight line through the origin with slope $\Delta\beta = (x - 1)\beta_{\text{eff}}$. Estimating that slope thus immediately allows us to compute β_{eff} .

Having computed β_{eff} , the freezeout point follows from a simple calculation. For this, we observe that using the operating temperature of D-Wave 2000Q of $T = 15$ mK, and the Boltzmann constant $k_B = 20.83661$ GHz/K, we can convert β_{eff} via $\beta_{\text{eff}}k_BT$ into a point on the anneal schedule $B(s)$ displayed in Fig. 1. Finding the s^* such that $B(s^*) = \beta_{\text{eff}}k_BT$ will yield the freezeout point.

The aforementioned method to measure the freezeout point is dependent on the choice of the parameter $x \in (0, 1)$ used to rescale the Hamiltonian. Typically, values of x too close to zero will cause the rescaled Hamiltonian to be too different from the original one (thus also causing its Boltzmann distribution to be too far away from the one of the unscaled Hamiltonian), whereas values of x too close to one will not yield a good separation of the rescaled and unscaled energy measurements used in (2). We typically choose x on a grid in the interval $[0.6, 0.95]$. After computing the freezeout points for each such x , in the experiments of Section 3 we report the measurement of the freezeout point corresponding to the largest value of $x < 1$.

2.4 Slicing an anneal schedule with a pause

In the experiments of Section 3, we also aim to investigate the effect of inserting a pause into the anneal process. Fig. 3 illustrates an annealing schedule that includes a pause (the black line), and a series of slicing schedules (green, red, and blue lines). Specifically, the annealing with

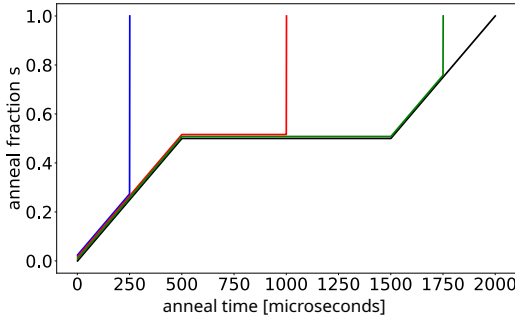


Figure 3: Anneal schedule with a pause of length 1000 microseconds inserted 500 microseconds into the anneal. Quenching (near-vertical jumps) at time points 250 (blue), 1000 (red), and 1750 (green) microseconds. The full anneal schedule is shown by the black line. Total anneal time of 2000 microseconds.

pause schedule in Fig. 3 starts with 500 microseconds regular anneal, at which a pause of 1000 microseconds is inserted. Afterwards, the normal anneal schedule is resumed until it reaches the total anneal time of 2000 microseconds. Slicing the anneal before and during the pause allows us to observe how the energy of the ground state evolves even while the Hamiltonian evolution is halted.

3 Experiments

This section presents our experimental setup and results. We start with an assessment of the tuning parameters of our genetic algorithm (Section 3.1). In Section 3.2, we present first results on the slicing technique of Section 2.1, demonstrating that the Ising model returned by Algorithm 1 indeed yields more pronounced changes during the anneal.

We then focus on how the energy (Section 3.3) and the Hamming distance (Section 3.4) of the ground state evolve during annealing.

Moreover, we look into a particular feature of the D-Wave 2000Q, the inclusion of a pause in the anneal process (Section 3.5). Since the instance returned by the genetic algorithm does not correspond to a known NP-hard problem, we modify Algorithm 1 to yield a QUBO for a well-known NP-hard problem, the Maximum Clique problem. We use this QUBO to investigate how the energy, Hamming distance, and freezeout point behave (Section 3.6). Our slicing technique allows us to define a quantity related to the freezeout point which we define in Section 3.7. Additionally, our slicing technique allows us to visualize how chain breaks occur during the anneal (Section 3.8), and we investigate individual freezeout points for all qubits (Section 3.9).

Apart from Section 3.2, which also displays results for a random Ising model, all figures in the remainder of the simulations were computed using an Ising model obtained with the genetic algorithm described in Section 2.2, or a modification thereof.

3.1 Parameter choices for the genetic algorithm

We start by assessing the dependence of the genetic algorithm described in Section 2.2 on its tuning parameters. For this we first define a set of default parameters: population size $N = 100$,

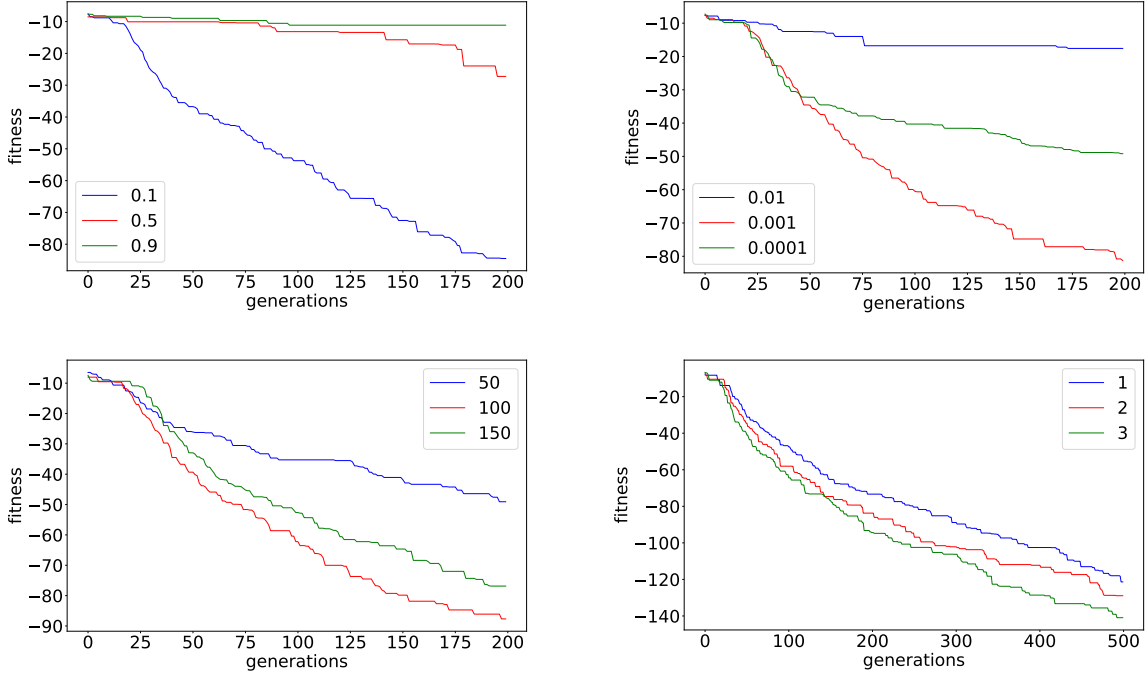


Figure 4: Dependence of the genetic algorithm on its tuning parameters while keeping the other parameters at their default values. Crossover proportion $p_{\text{cross}} \in \{0.1, 0.5, 0.9\}$ (top left), mutation rate $p_{\text{mut}} \in \{0.0001, 0.001, 0.01\}$ (top right), and population size $N \in \{50, 100, 150\}$ (bottom left). Bottom right shows three runs of the genetic algorithm with the optimized parameters.

crossover proportion $p_{\text{cross}} = 0.1$, and mutation rate $p_{\text{mut}} = 0.001$.

While keeping two of the default parameters fixed, we vary the third parameter in Figure 4. Figure 4 shows that selecting a low crossover rate ($p_{\text{cross}} = 0.1$) seems to be advantageous. However, choosing the population size or the mutation rate to be too low or too high is disadvantageous, thus leading us to the choices $N = 100$ and $p_{\text{mut}} = 0.001$. The default parameters will be used in the remainder of the simulations. Figure 4 (bottom right) shows three runs of the genetic algorithm with default parameters for 500 generations, demonstrating a stable behavior of the tuned algorithm. When tuning a problem instance with our genetic algorithm in the following sections, we will always employ Algorithm 1 with 200 generations (iterations).

3.2 Evolution of ground state for two types of Ising models

We verify that using an Ising model computed with the genetic algorithm (Algorithm 2.2) is indeed advantageous for investigating the evolution of the ground state during the anneal. We refer to the optimized Ising model returned by Algorithm 1 as simply the *Chimera Ising* in the remainder of the text. To be precise, we employ the highest fitness Ising model from the third run of the genetic algorithm which is displayed in the lower right panel in Figure 4 as a green line.

Figure 5 shows, for 1000 slices (i.e., a 1000 microsecond anneal), the progression of the average of the 1 percent minimum energies found. We observe that the total change in energy is considerably more pronounced for the Chimera Ising returned by Algorithm 1 compared to

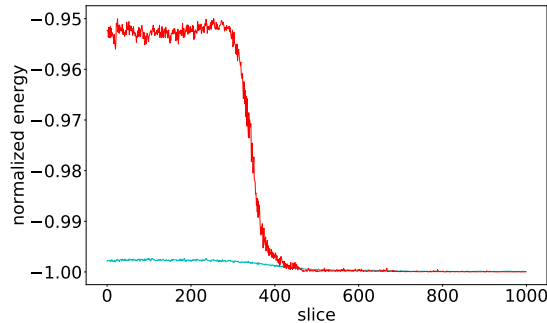


Figure 5: Averages of the minimum 1 percent energies found in 10 runs of 1000 anneals. Randomly generated and unstructured Ising model (cyan) and the Chimera Ising model (red). Both datasets are normalized by dividing each value by their respective minimum value.

a randomly generated non-optimized and unstructured Ising. Looking at the plot it seems straightforward to define the freezeout point to occur at roughly slice 500 where both curves stabilize horizontally. We will investigate the relationship between the point at which the energies stabilize in the slicing plots and the freezeout point computed with the methodology of [2] (see Section 2.3) in more detail in the next subsection.

3.3 Energy evolution during the anneal process

We now look at the evolution of energies for the Chimera Ising model. In this and all following sections, we always slice an anneal process using 1000 and 2000 slices. Since we slice in steps of one microsecond, the figures showing 1000 slices are always computed for a total anneal time of 1000 microseconds, and the figures showing 2000 slices have a total anneal time of 2000 microseconds. For each slice we run 1000 anneals on D-Wave 2000Q. In the plots, we report both the mean energy among all samples returned by D-Wave 2000Q as well as the average best 1% energies, that is the mean among the 1% lowest energies observed among the 1000 samples. The Hamming distance we report is the average distance among the bitstrings corresponding to the 1% best (lowest energy) samples.

Figure 6 displays results for the Chimera Ising model of Algorithm 1 with 1000 and 2000 slices. We observe that, initially, the energies roughly stay constant up to around a third of the anneal time. At that point, a continuous reduction in energies sets in, during which the ground state energy becomes better and better with every slice. Roughly halfway through the anneal the energies stabilize.

We applied the freezeout point estimation algorithm described in Section 2.3, but it failed to produce a freezeout point value neither for 1000 nor for 2000 slices, which indicates that the distribution of the samples' energies doesn't follow a Boltzmann distribution.

3.4 Evolution of the Hamming distance between adjacent slices

Similarly to Figure 6, we record the Hamming distance between the binary solution vectors (indicating the final measured value of each qubit) of adjacent slices, thus measuring in how many bits the solution vectors of adjacent slices differ.

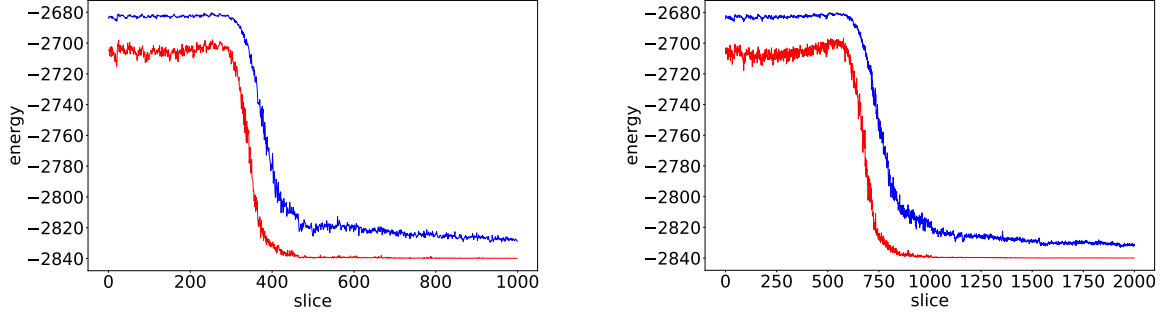


Figure 6: Evolution of minimum energy states on the D-Wave 2000Q for 1000 slices (left) and 2000 slices (right). Mean of all samples (blue) and mean of the lowest 1% energies (red).

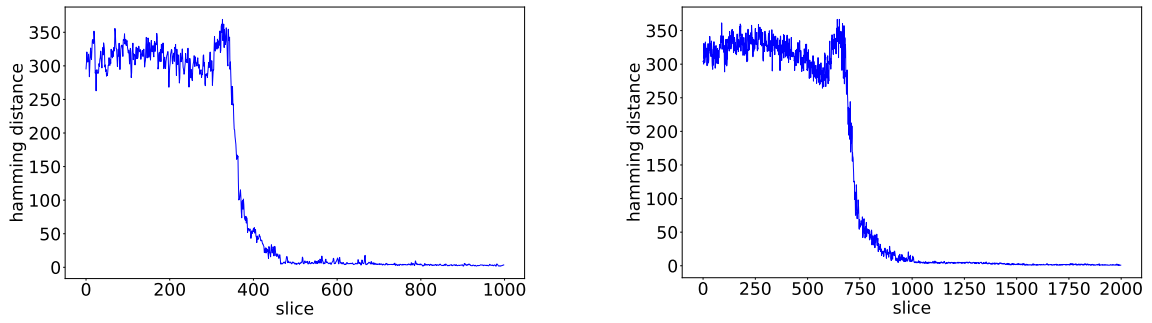


Figure 7: Evolution of the Hamming distance for the ground states between adjacent slices. Plots show 1000 slices (left) and 2000 slices (right).

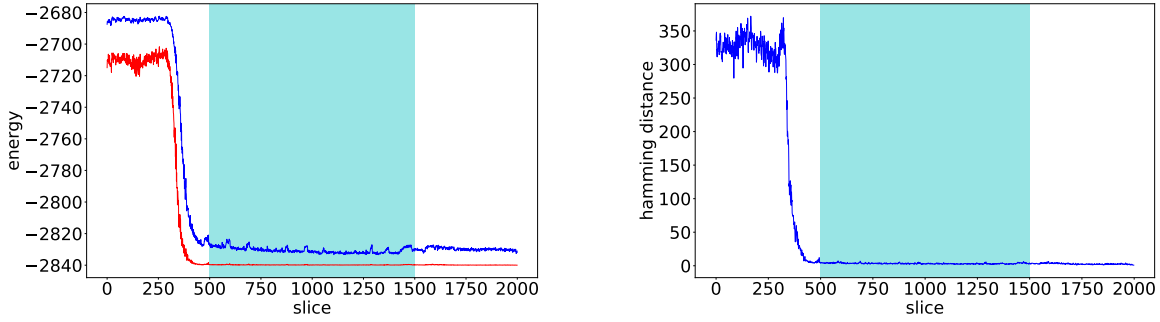


Figure 8: Evolution of energies (left) and Hamming distance (right) during a 2000 microsecond anneal with a 1000 microsecond pause. The pause was inserted at the lower bound of the freezeout point measurement from Figure 6. Pause location is shaded in cyan from 500 to 1500 microseconds.

Figure 7 shows the evolution of the Hamming distance for the ground states between adjacent slices for 1000 and 2000 microsecond anneals. Interestingly, the shapes of the curves are similar for the two anneal durations, and importantly they coincide with the shape of the progression of energies in Figure 6. However, the cause of the slight uptick in Hamming distance before the pronounced decrease is unknown.

3.5 Pausing the anneal

We are interested in investigating how the ground state progresses when the anneal is paused. In particular, we are interested in observing if the ground state continues to evolve after the freezeout has occurred, measured as before in terms of the mean and average best (lowest) 1% energies as well as Hamming distance.

For this we select the schedule displayed in Figure 3: it has a total anneal time of 2000 microseconds, with a pause inserted at slice 500 out of 1000 slices (microseconds). The pause duration was 1000 microseconds.

Figure 8 shows results of this experiment. We observe that, as before, both the energy and Hamming distance of the ground states continue to decrease during the pause, which is shaded in light blue. Surprisingly, as soon as the pause is over, we observe a slight uptick in the energy measurements, which then quickly stabilize again towards the end of the 2000 microsecond anneal. The reason of this behavior is unknown, but it could be related to an artifact caused by the D-Wave annealer.

3.6 Energy evolution for the Maximum Clique problem

We are interested in peering into the anneal process not only for arbitrary (unstructured) Ising problems that conform to the Chimera topology, but also for ones that correspond to classic NP-hard problems. An important feature of such problems is that they should, before annealing, be minor-embedded in the Chimera graph, which means they have chains, sets of strongly coupled physical qubits, corresponding to a logical qubit. Chained problems are believed to have a different behavior (are generally more difficult for quantum annealing) compared to the unchained ones. To this end, we select an important NP-hard problem, the Maximum Clique

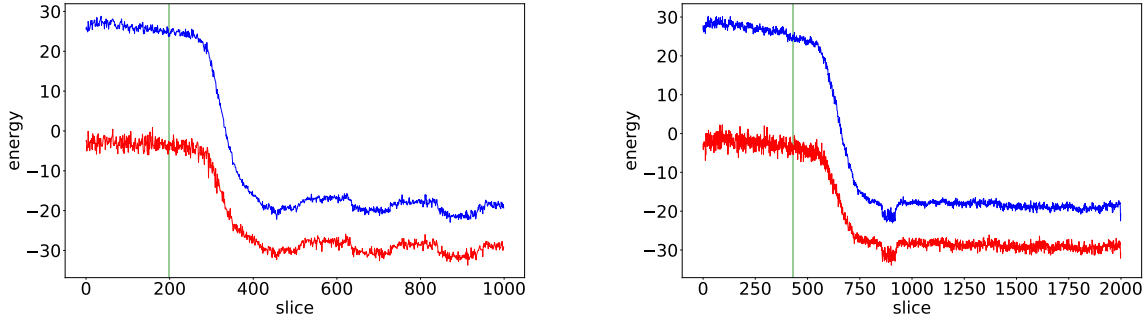


Figure 9: Evolution of energies for the optimized Maximum Clique QUBO using 1000 slices (left) and 2000 slices (right). Mean of all samples (blue) and mean of the lowest 1% energies (red). Freezeout point shaded in green.

problem [9], for analyzing with our slicing method. Since the QUBO for the Maximum Clique problem is of a special form, we employ a modification of Algorithm 1 for the optimization, using 200 generations. In particular, we start with an initial population of Maximum Clique QUBOs, and every time a crossover or mutation step is performed, we directly work on the edges of the graph for which the Maximum Clique problem is computed. This ensures that, after crossover and mutation, the population of QUBOs continues to contain only those QUBOs that actually correspond to a Maximum Clique problem. In this way, we can find a QUBO of type (1) that corresponds to an actual Maximum Clique problem, while also ensuring a large difference between the energies for $1 \mu\text{s}$ and $1000 \mu\text{s}$ anneals, thereby reducing the distortion caused by quenching.

To sample initial graphs $G = (V, E)$ for which the Maximum Clique problem is solved, we draw random graphs with $|V| = 65$ vertices and a density (edge probability) that is uniformly sampled in $[0.2, 0.8]$. When embedding the resulting Maximum Clique QUBOs, we employ a fixed chain strength of 2. When running the genetic algorithm, we employ the default choices of Section 3.1, apart from setting $p_{\text{mut}} = 0.01$ due to the fact that we have a smaller number of parameters in this setting.

Figure 9 shows an interesting behavior of the Maximum Clique QUBO returned by the modified Algorithm 1. As seen before, at the beginning of the anneal, both the energies as well as the Hamming distance between adjacent slices slightly decrease before the pronounced decrease sets in. Notably, there seems to be some sort of minimum right after this pronounced decrease for both energy and Hamming distance, and the energy measurements for the QUBO continue to be volatile (oscillatory).

We computed a freezeout point using the algorithm in Section 2.3, and observe that the result indicates that the freezeout occurs earlier than suggested by our slicing plots. Note that if the quenching used by our slicing algorithm modifies the position in the slicing plot where the energy evolution will become negligible, i.e., the freezeout point position, it will move it to an earlier point, but not to a later one. This means that the discrepancy in the position of the freezeout point is due mostly to inaccuracies in the algorithm from Section 2.3, since the slicing algorithm can only underestimate the freezeout position, but not overestimate it.

Similarly to Figure 9, Figure 10 displays the evolution of the Hamming distance between

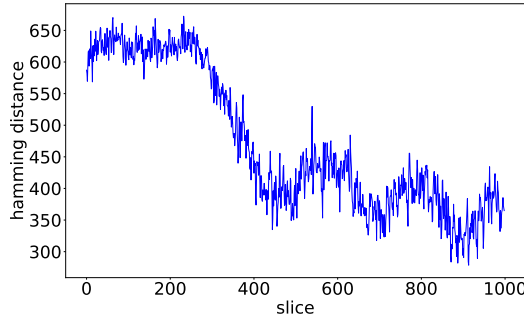


Figure 10: Evolution of the Hamming distance for the Maximum Clique QUBO using 1000 slices.

adjacent slices during a 1000 microsecond anneal. We observe that, similarly to the energy evolution in Figure 9, the Hamming distance first stays relatively constant before a pronounced drop occurs. Two observations are noteworthy. First, we again observe a minimum after the drop. Second, we observe even more pronounced oscillations than in the energy measurement case.

3.7 Quasi-freezeout point

We observed in the previous subsections that each of the shapes of the energy evolution plots follows roughly the same pattern: After an initial phase, in which the current ground state stays mostly constant (Phase 1), a pronounced decline sets in (often at around one third of the anneal time). This phase of the steep decline (Phase 2) roughly lasts until about halfway during the anneal, after which the energies stabilize quickly. This is followed by Phase 3, which consists of a relatively long stretch of time until the end of the anneal, in which the energy is roughly constant or is decreasing very slowly. Assuming the slope of the line that approximates the energy slicing plot of this phase is not too steep, in terms of a user specified threshold, we call the point of the anneal process at which the third phase starts a *quasi-freezeout point (QFP)*.

In order to break down the energy slicing plot into the three main phases described above, we fit a polyline (degree-one spline) using the Bayesian Optimization package of [13], that consists of three main segments, corresponding to the three phases, and possibly a small number of shorter connecting segments, depending on the graph, to each slicing energy plot. Figure 11 shows results of our fit. We consider both the Chimera Ising model of Section 3.2 and the Maximum Clique problem of Section 3.6, obtained with Algorithm 1.

Fitting a spline to the slicing energies gives our method two advantages: First, if the slope of the third segment is not significantly different from zero, we conclude that the system has not frozen out prior to the end of the anneal. This will correspond to the case where a freezeout point does not exist for the system. The existence of a QFP can be made dependent on a threshold for the slope set by the user, which typically varies based on the problem being solved, the annealer hardware, and the purpose of the analysis. In our case, we consider a system "frozen out" if the slope of the last spline segment is less than 10 degrees.

Second, if indeed the slope of the third segment is zero (i.e., not significantly different from zero), or less than the user-defined threshold, then we conclude that the freezeout must have

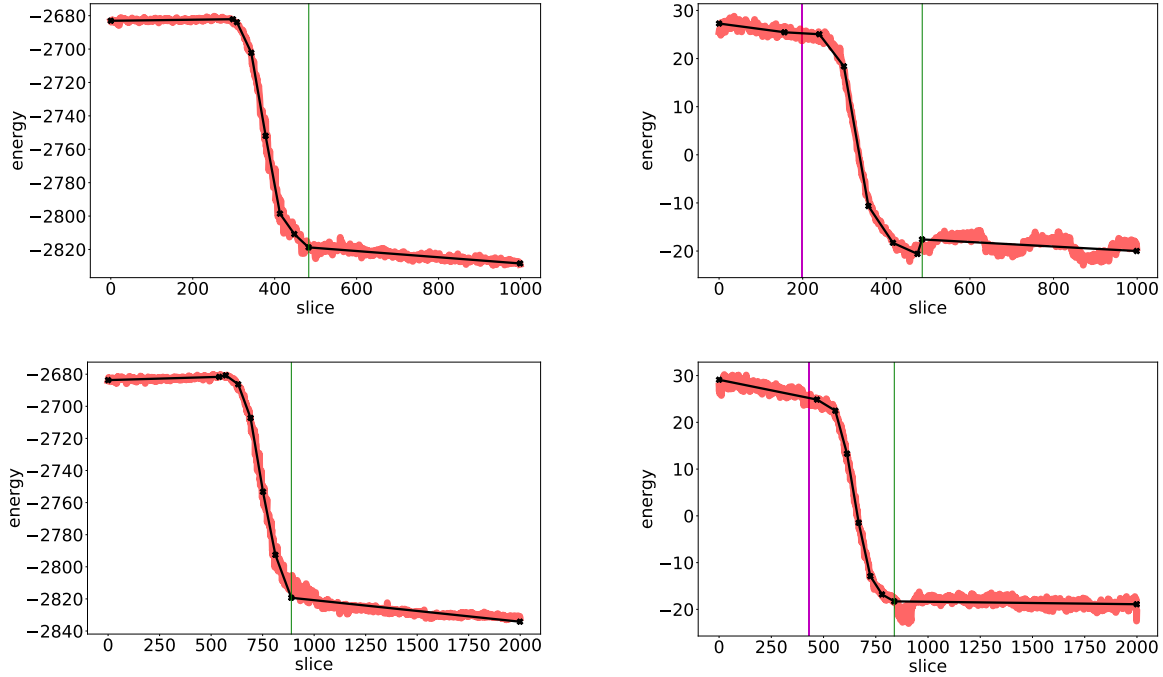


Figure 11: Chimera Ising problem (top left) and Maximum Clique problem (top right), both with anneal duration $1000 \mu\text{s}$ and found using Algorithm 1. The same problems, but with anneal duration $2000 \mu\text{s}$, are shown in the bottom row. Green vertical lines show the QFP found by the spline method. Magenta vertical lines show the freezeout points computed by the method from Section 2.3 (that method could not find any freezeout point for the Chimera Ising problem).

occurred at the intersection of the penultimate and ultimate segment, that is, the point at which the third segment begins. In this case, we can use the QFP as an approximation of the freezeout point.

In Figure 11, we examine the QFP found for two problems: the Chimera Ising model from 3.2 (i.e., not corresponding to any particular NP-hard problem), and the one for the Maximum Clique problem from 3.6. Both are found with Algorithm 1. We display the fitted spline segments, and indicate the QFP determined by the last spline with a green line. Additionally, we compute the freezeout point with the method of Section 2.3. We observe that for the Chimera Ising problem, the technique of [2] does not work, and that it finds a freezeout point which seems to occur before the point at which the energies stabilize for the Maximum Clique problem (purple vertical lines, right column). The QFP is indicated with a vertical green line and could be a sensible indicator for the freezeout location.

The 3-tuple of the slopes of the three segments corresponding to Phases 1, 2, and 3, together with the QFP, could be possibly used as a signature vector characterizing the anneal evolution for each problem. Since we have looked at only two problems, we cannot suggest any rules that link such a signature with characteristics of individual problem, but it may be a topic of future research.

The precise slope estimates (in degrees) for the three slopes in each of the subfigures of Figure 11 can be found in Table 1.

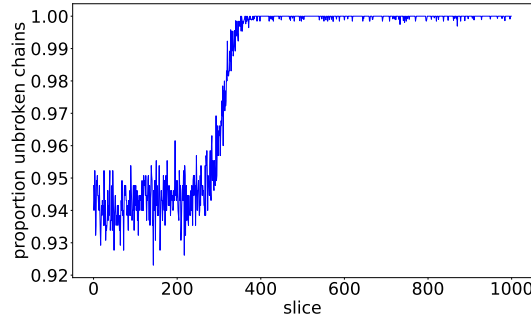


Figure 12: Proportion of unbroken chains for the Maximum Clique QUBO using 1000 slices.

Problem	anneal time	Phase 1	Phase 2	Phase 3
Chimera Ising	1000 μs	3.45	-84.21	-7.07
Chimera Ising	2000 μs	3.0	-84.54	-9.71
Maximum Clique	1000 μs	-16.92	-84.42	-2.32
Maximum Clique	2000 μs	-17.46	-84.3	-1.31

Table 1: Spline segment slopes (in degrees) for Figure 11

3.8 Proportion of chain breaks

Our slicing technique allows us to also look at the progression of individual qubits during the anneal (see Section 3.9). In particular, for the Maximum Clique QUBO we can investigate how its chains on the D-Wave chimera graph evolve.

Figure 12 displays the proportion of unbroken chains (where an unbroken chain is defined as a chain whose qubits all take the same value) as a function of the anneal slice for a 1000 microsecond anneal. We observe that initially, up to around one third of the anneal, roughly 95% of all chains are unbroken. Towards one third of the anneal time, roughly coinciding with the drop in energies, all of the chains become unbroken.

3.9 Determining quasi-freezeout points at individual-qubits level

We can use our methodology from Section 2.1 to track when individual qubits of D-Wave “freeze” during the anneal. To this end, we again employ the Ising or QUBO model obtained with the genetic algorithm of Section 2.2, and read out the value of each qubit at each of the 1000 slices during a 1000 microsecond anneal.

In this way, we can track from what slice onwards the value of each of the qubits remained in the state it was upon readout at the full anneal duration. We define this timepoint as the *quasi-freezeout point (QFP)* for that individual qubit. The bitstrings we query for each slice are the ones corresponding to the best energy.

Figure 13 shows results of this experiment for the Chimera Ising (having 2032 variables) and the Maximum Clique problems (having 1555 variables) obtained with Algorithm 1. Each of the two histograms shows the number of qubits that freeze out at a particular point in time (or slice number) during the anneal.

We observe that, for the Chimera Ising model, the histogram correlates with the slicing diagrams we have seen earlier. In particular, at the start of the anneal, not many qubits freeze

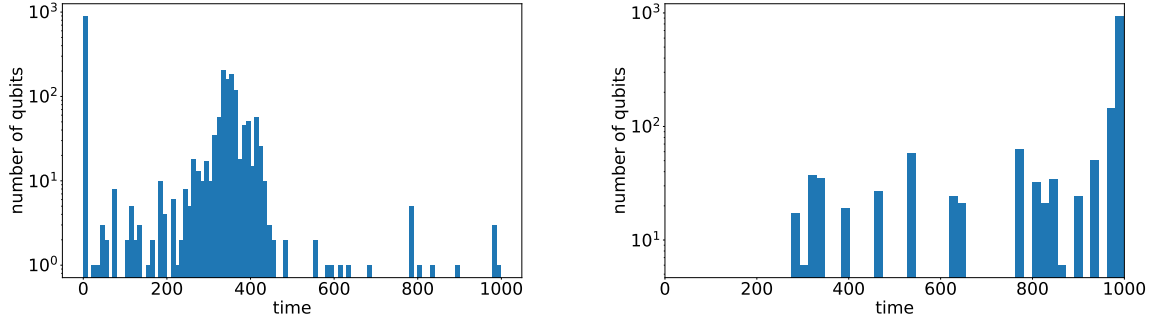


Figure 13: Histograms showing the number of frozen out qubits at each slice. Left histogram shows the Chimera Ising model, and right histogram shows the Maximum Clique problem, obtained with Algorithm 1.

out. Roughly at one third of the anneal duration, when we observe the pronounced decrease in the slicing energies, a majority of qubits freeze out. The one exception, which, on the surface, doesn't make sense, is the large number (≈ 900) of qubits that have frozen out at slice 1. Actually, this gives out some useful information, since these qubits must have frozen because of the quench—they have attained their optimal values as a result of the quench done as part of the slicing at $1 \mu s$ time. It cannot be explained by the $1 \mu s$ anneal that precedes that quench because, at $s = 0.001$, the value of the function $B(s)$ from Figure 1 is practically zero, so the annealer doesn't have enough information about the QUBO or Ising model (1) in order to compute these optimal values. Hence, we can conclude that the distortion caused by the the quenches is expressed by having the values of ≈ 900 qubits fixed, while the remaining ≈ 1100 qubits determine the reduced QUBO or Ising model whose anneal progression we observe on the slicing diagrams for the Chimera Ising problem.

For the Maximum Clique problem, the histogram on the right of Figure 13 tells a different story. No qubit freezes out before slice 275, and after that, qubits freeze out at a roughly uniform rate almost until the end of the anneal. This is consistent with the slicing diagram, which show that the ground state energy keeps on decreasing slowly until the end of the anneal. The increased number of frozen qubits at the very end is due to the fact that the annealing is soon ending and there is not enough time (slices) to allow for the qubits to flip again. The fact that the qubits freezeout times are spaced out with longer intervals between them, and that several qubits freeze out at the same time is due to the chained nature of the Maximum Clique problem. Qubits representing a logical qubit are chained together, so typically it is either a logical qubit flipping, or a part of a broken chains flips. Finally, the lack of frozen qubits at slice 1 indicates that, for the Maximum Clique problem, the quench didn't result in such a big distortion as it happened for the Chimera Ising problem, and the slicing result is more reliable. On the other side, the slicing diagrams for both problems have similar shapes, which may indicate that, despite the distortion caused by the quench, the Chimera Ising plots still yield useful information.

4 Discussion

This article is a first attempt to explore how the ground state of a quantum annealer evolves during the anneal process. To the best of our knowledge, such work has not been presented previously in the literature.

In order to estimate the states of individual qubits at any point during the anneal, we develop a novel method we refer to as slicing, which uses the D-Wave 2000Q quenching control feature. Using this technique, we dissect the anneal process and monitor how the ground state energy evolves. These slicing plots also allow us to track when energies or qubit flips stabilize during the anneal, which can be used as an alternative technique to approximate the freezeout point, similarly to the methodology of [2].

We summarize our findings as follows:

1. We demonstrate that using an optimized Ising or QUBO model computed with a genetic algorithm results in a much more pronounced evolution during the anneal than using a random problem instance.
2. Using optimized Ising or QUBO models, we observe that ground state evolution follows in all cases a similar pattern. Initially, the energy does not considerably decrease during the anneal. At roughly a quarter of the anneal, a pronounced decrease sets in, which correlates with a reduction in the number of bit flips. At around the midpoint of the anneal, the energy stabilizes at around the energy value that D-Wave returns as a solution at the end of the anneal. During that phase, the number of bit flips likewise stabilizes at a constant level (meaning that the ground state still changes from slice to slice), which could reflect the noise in the machine.
3. Our technique provides an alternative to approximately determine the freezeout point, together with methods such as the one of [2]. We introduce the notion of a quasi-freezeout point based on the data collected during slicing, which can be used to approximate the freezeout point in cases it cannot be computed by other methods, and suggested an algorithm for its computation.
4. We demonstrate that the ground state still keeps on evolving even during a pause in the anneal process.
5. For the case of Maximum Clique problem, we show that the proportion of broken chains is low at the start of the anneal and quickly decreases to zero, meaning that all chains are unbroken early on in the anneal.
6. We show that the Chimera Ising and the Maximum Clique problem have quite different behaviors. While, in the former, a large number of qubits freeze very early during the anneal, for the latter no qubits freeze out during the first quarter of the anneal, after which qubits obtain their final values at roughly the same rate until the end of the anneal.

This work serves as a first step in the development of methods that would allow us to get further insights into the (unobservable) anneal process. Indeed, a multitude of further avenues of research are possible:

1. Improving the genetic algorithm implementation by including possibly advantageous characteristics of genetic algorithms such as multiple individual crossovers, adaptive mutation and crossover rates, and different types of elitism.
2. Slicing problems using other types of anneal schedules such as reverse annealing schedules.
3. Slicing other interesting problems, including chained optimization problems such as Maximum Cut and Graph Partitioning, and problems that are especially difficult for D-Wave to solve.
4. Investigate for random Ising problems if the set of D-Wave qubits that freeze out early/late changes. If we consistently observe the same qubits freezing out early/late, we might deduce biases or other properties of the D-Wave machine.
5. Finally, if future hardware or software advances allow quenching time to become much shorter, e.g., in the low nano-second range, the methods proposed here will be able to produce more accurate results.

Acknowledgment

This work was supported by the US Department of Energy through the Los Alamos National Laboratory and by the Laboratory Directed Research and Development program of Los Alamos National Laboratory under project numbers 20190065DR and 20180267ER. Los Alamos National Laboratory is operated by Triad National Security, LLC, for the National Nuclear Security Administration of U.S. Department of Energy (Contract No. 89233218CNA000001).

References

- [1] Mohammad H. Amin. Searching for quantum speedup in quasistatic quantum annealers. *Phys. Rev. A*, 92:052323, Nov 2015.
- [2] Marcello Benedetti, John Realpe-Gómez, Rupak Biswas, and Alejandro Perdomo-Ortiz. Estimation of effective temperatures in quantum annealers for sampling applications: A case study with possible applications in deep learning. *Phys Rev A*, 94(022308), 2016.
- [3] Guillaume Chapuis, Hristo Djidjev, Georg Hahn, and Guillaume Rizk. Finding Maximum Cliques on the D-Wave Quantum Annealer. *Journal of Signal Processing Systems*, 91(3-4):363–377, 2019.
- [4] D-Wave Systems. Quantum Computing for the Real World Today, 2017.
- [5] D-Wave Systems. QPU Properties: D-Wave 2000Q System at LANL, 2019.
- [6] D-Wave Systems. Technical Description of the D-Wave Quantum Processing Unit, 2020.
- [7] D-Wave Systems. Practical Quantum Computing – D-Wave Technology Overview, 2020.
- [8] E. D. Dahl, D-Wave Systems. Programming with D-Wave: Map coloring problem, 2013.

- [9] A. Lucas. Ising formulations of many NP problems. *Front Phys*, 2(5):1–27, 2014.
- [10] Jeffrey Marshall, Eleanor G. Rieffel, and Itay Hen. Thermalization, freeze-out, and noise: Deciphering experimental quantum annealers. *Phys. Rev. Applied*, 8:064025, Dec 2017.
- [11] Jeffrey Marshall, Davide Venturelli, Itay Hen, and Eleanor G. Rieffel. Power of pausing: Advancing understanding of thermalization in experimental quantum annealers. *Phys. Rev. Applied*, 11:044083, Apr 2019.
- [12] Melanie Mitchell. *An Introduction to Genetic Algorithms*. MIT Press, Cambridge, MA, USA, 1996.
- [13] Fernando Nogueira. Bayesian Optimization: Open source constrained global optimization tool for Python, 2014–.
- [14] Masaki Ohkuwa, Hidetoshi Nishimori, and Daniel A. Lidar. Reverse annealing for the fully connected p-spin model. *Phys. Rev. A*, 98(2):022314, 2018.
- [15] G. Passarelli, V. Cataudella, and P. Lucignano. Improving quantum annealing of the ferromagnetic p -spin model through pausing. *Phys. Rev. B*, 100:024302, Jul 2019.
- [16] E. Pelofske, G. Hahn, and H. Djidjev. Peering into the anneal process of a quantum annealer. In *20th International Conference on Parallel and Distributed Computing, Applications and Technologies (PDCAT)*, pages 184–189, 2019.
- [17] Elijah Pelofske, Georg Hahn, and Hristo Djidjev. Optimizing the spin reversal transform on the D-Wave 2000Q. In *2019 IEEE International Conference on Rebooting Computing (ICRC)*, pages 1–8. IEEE, 2019.
- [18] Elijah Pelofske, Georg Hahn, and Hristo Djidjev. Solving large maximum clique problems on a quantum annealer. In *Proceedings of the First International Workshop on Quantum Technology and Optimization Problems, QTOP, Munich, Germany, March 18, 2019*, pages 123–135, 2019.
- [19] Elijah Pelofske, Georg Hahn, and Hristo Djidjev. Solving large minimum vertex cover problems on a quantum annealer. In *Proceedings of the 16th ACM International Conference on Computing Frontiers, CF 2019, Alghero, Italy, April 30 - May 2, 2019.*, pages 76–84. ACM, 2019.
- [20] Elijah Pelofske, Georg Hahn, and Hristo Djidjev. Advanced anneal paths for improved quantum annealing. In *IEEE International Conference on Quantum Computing and Engineering*. IEEE, 2020.